Ann. Geophys., 33, 941–953, 2015
www.ann-geophys.net/33/941/2015/
doi:10.5194/angeo-33-941-2015

Annales Geophysicae
Open Access

A case study on generation mechanisms of a sporadic sodium layer above Tromsø (69.6° N) during a night of high auroral activity

T. Takahashi[1,2], S. Nozawa[1], T. T. Tsuda[3,4], Y. Ogawa[4,5], N. Saito[6], T. Hidemori[1], T. D. Kawahara[7], C. Hall[8], H. Fujiwara[9], N. Matuura[1], A. Brekke[10], M. Tsutsumi[4,5], S. Wada[6], T. Kawabata[1], S. Oyama[1], and R. Fujii[1]

[1]Solar-Terrestrial Environment Laboratory, Nagoya University, Nagoya, Japan
[2]Center for Space Science and Radio Engineering, The University of Electro-communications, Chofu, Tokyo
[3]Department of Communication Engineering and Informatics, The University of Electro-communications, Chofu, Tokyo
[4]National Institute of Polar Research, Tachikawa, Tokyo, Japan
[5]Graduate University for Advanced Studies, Tokyo, Japan
[6]RIKEN Center for Advanced Photonics, RIKEN, Wako, Saitama, Japan
[7]Faculty of Engineering, Shinshu University, Nagano, Nagano, Japan
[8]Tromsø Geophysical Observatory, The Arctic University of Tromsø, Tromsø, Norway
[9]Faculty of Science and Technology, Seikei University, Musashino, Tokyo, Japan
[10]Faculty of Science, The Arctic University of Tromsø, Tromsø, Norway

Correspondence to: T. Takahashi (ttohru@stelab.nagoya-u.ac.jp)

Received: 15 January 2015 – Revised: 7 May 2015 – Accepted: 19 June 2015 – Published: 5 August 2015

Abstract. We have quantitatively evaluated generation mechanisms of a sporadic sodium layer (SSL) based on observational data obtained by multiple instruments at a high-latitude station: Ramfjordmoen, Tromsø, Norway (69.6° N, 19.2° E). The sodium lidar observed an SSL at 21:18 UT on 22 January 2012. The SSL was observed for 18 min, with a maximum sodium density of about 1.9×10^{10} m^{-3} at 93 km with a 1.1 km thickness. The European Incoherent Scatter (EISCAT) UHF radar observed a sporadic E layer (Es layer) above 90 km from 20:00 to 23:00 UT. After 20:00 UT, the Es layer gradually descended and reached 94 km at 21:18 UT when the SSL appeared at the same altitude. In this event, considering the abundance of sodium ions (10 % or less), the Es layer could provide only about 37 % or less of the sodium atoms to the SSL. We have investigated a temporal development of the normal sodium ion layer with a consideration of chemical reactions and the effect of the (southwestward) electric field using observational values of the neutral temperature, electron density, horizontal neutral wind, and electric field. This calculation has shown that those processes, including contributions of the Es layer, would provide about 88 % of sodium atoms of the SSL. The effects of meteor absorption and auroral particle sputtering appear to be less important. Therefore, we have concluded that the major source of the SSL was sodium ions in a normal sodium ion layer. Two processes – namely the downward transportation of sodium ions from a normal sodium ion layer due to the electric field and the additional supply of sodium ions from the Es layer under relatively high electron density conditions (i.e., in the Es layer) – played a major role in generating the SSL in this event. Furthermore, we have found that the SSL was located in a lower-temperature region and that the temperature inside the SSL did not show any remarkable temperature enhancements.

Keywords. Ionosphere (auroral ionosphere)

1 Introduction

A sporadic sodium layer (SSL), first reported by Clemesha et al. (1978) in São Paulo, Brazil (23° S, 46° W), is a dense thin sodium layer superposed on a normal sodium layer. Major characteristics of SSLs would be summarized as follows: (1) there is a large difference in vertical and horizontal distribution; (2) there is a high ratio of peak sodium density to background normal sodium density; and (3) SSLs experi-

ence rapid growth and an extended life span. SSLs typically have a thin vertical extent with a full width at half maximum (FWHM) of 1–2 km (e.g., Batista et al., 1989; Clemesha et al., 1999). On the other hand, the typical horizontal extent is between about 100 and 300 km (cf. Batista et al., 1991; Fan et al., 2007). Clemesha et al. (1999) mentioned that the median value was about 420 km as a typical horizontal dimension at São Jose dos Campos. SSLs that extended farther than 1000 km were also observed by an airborne lidar (e.g., Kane et al., 1991; Gu et al., 1995; Qian et al., 1998). SSLs have concentrations about 2–10 times higher than that of the background normal sodium layer (cf. Nagasawa and Abo, 1995; Simonich, 2005). For example, a typical sodium density at 95 km in winter is about $3 \times 10^9\,\mathrm{m}^{-3}$, and typical SSLs may have concentrations of about $2 \times 10^{10}\,\mathrm{m}^{-3}$ at the same altitude (Clemesha, 1995). SSLs typically reach their maximum concentration at an interval between 2 and 20 min and last for a few tens of minutes to several hours (e.g., Cox and Plane, 1998; Batista et al., 1989).

Generation mechanisms of SSLs have been discussed for more than 3 decades but questions remain. Proposed mechanisms are as follows: direct meteor deposition, release from aerosol particles, chemical reduction of appropriate metal compounds, redistribution of existing atoms, and recombination of ions (Clemesha et al., 1999). There may be two candidates for the source of sodium atoms: one is neutral sodium-bearing molecules and atoms and the other is sodium ions. For example, the altitudinal redistribution of sodium atoms has been proposed as one of the major generation mechanisms of SSLs by Clemesha (1995). Kirkwood and von Zahn (1991) proposed a generation mechanism in which a concentration of metallic ions transported downward by electric fields could generate an SSL at high latitudes. In the first report of an SSL, Clemesha et al. (1978) suggested that the origin of the excess sodium atoms must be due to meteor deposition, and in a later paper Clemesha et al. (1988) suggested a mechanism whereby an initially thick layer caused by meteor deposition could be converted into a thin layer by wind shear. This mechanism requires a large meteor and/or a large meteor shower with a total mass greater than 100 kg, but it is believed that occurrence of such a meteor event is rare (Keay and Ceplecha, 1994). By using model calculations, Plane (2004) proposed that sodium atoms in the topside of a normal sodium layer are in equilibrium with sodium ions through several chemical reactions. Among sodium compound ions, NaN_2^+ contributes greatly to the generation of sodium atoms. Since chemical reactions of NaN_2^+ are sensitive to the background temperature, an investigation of the background temperature is also important for understanding of the generation mechanisms. Chemical reactions show an inverse correlation between sodium atom production and the background temperature (Plane, 2004). On the other hand, based on observations, Zhou et al. (1993) argued that a temperature increase due to tide and/or gravity wave may produce a sodium enhancement. Gardner et al. (1993) reported that there was a temperature enhancement over 40 K inside an SSL. Based on 43 SSL events obtained during the Airborne Lidar and Observations of Hawaiian Airglow/Airborne Noctilucent Cloud (ALOHA/ANLC-93) campaigns, Qian et al. (1998) reported that the majority of the SSLs had considerably higher temperatures than the mean; the average temperature enhancement was about 13 K. Therefore, the importance and role of the temperature in generating SSLs are controversial (cf. Delgado et al., 2012). It should be pointed out that due to quick temporal and large altitudinal variations in the sodium density inside an SSL (cf. Liu and Yi, 2009), the derivation of the temperature requires a high-performance lidar system.

Sodium atoms can be sputtered by energetic auroral particles from dust particles (von Zahn and Hansen, 1988). Though Hansen and von Zahn (1990) dismissed this idea because of the poor correlation between sodium densities and cosmic noise absorption measured by a riometer, Gu et al. (1995) proposed that the aurora was the cause of the SSL formation because an SSL and an aurora seemed to be colocated in space. On the other hand, Tsuda et al. (2013) clearly showed the anticorrelation of sodium number densities and auroral particle precipitation based on simultaneous observations of the sodium lidar and European Incoherent Scatter (EISCAT) VHF radar at Ramfjordmoen, Tromsø. Therefore, the role of auroral particle precipitation in generating an SSL is controversial.

A sporadic E layer (Es layer) is an appearance of an unusual plasma layer in the upper-mesosphere and lower-thermosphere (MLT) region (Whitehead, 1989; Mathews, 1998). Since Es layers consist of metal ions (Fe^+, Mg^+, Na^+, etc.), it has been thought that Es layers would play an important role in generating SSLs. High correlations between the occurrence of SSLs and Es layers have been reported (cf. von Zhan et al., 1987; von Zhan and Hansen, 1988; Nagasawa and Abo, 1995). A problem with this idea is a low abundance (about 10 % or less) of sodium ions in Es layers (cf. Clemesha et al., 1999). Heinselman (2000) reported, however, that an SSL could form via the chemical reactions proposed by Cox and Plane (1998) and that an Es layer could supply enough sodium atoms to generate the SSL. Es layers have been recently considered as the most likely candidate for the generation mechanisms of an SSL (cf. Clemesha et al., 1999; Yuan et al., 2014). However, SSLs were rarely observed at midlatitudes where the occurrence of Es layers is greater than at low and high latitudes (cf. Arras et al., 2008; Wu et al., 2005). This implies that SSLs cannot be generated by Es layers alone. Matuura et al. (2013) proposed the horizontal redistribution of ions as a new mechanism capable of providing a sufficient reservoir necessary for the formation of Es layers and subsequent metallic atom layers.

Existing observations suggest that different processes may be involved, depending on the latitude and altitude of the event (Qian et al., 1998). Contrary to studies of SSLs ob-

served at low latitudes, not much work has been conducted using an incoherent scatter (IS) radar and a sodium temperature lidar to investigate generation mechanisms of SSLs at high latitudes. In this paper, we have evaluated generation mechanisms of an SSL appearing in the polar MLT region on the night of 22 January 2012 by using data obtained with the sodium–temperature lidar, the EISCAT UHF radar, the meteor radar, an all-sky digital camera, and the three-wavelength photometer operated at the same observational field. Such a study using comprehensive data sets (in particular, simultaneous observations of a common volume of an IS radar and a sodium temperature lidar) is, as far as we know, conducted for the first time at high latitudes. The 3-hour Kp index was 4+, 4−, 5−, and 5− between 15:00 UT on 22 January and 03:00 UT on 23 January 2012. The aurora activity was high throughout the night. Conditions resembled those of the event reported by Heinselman et al. (1998) and Heinselman (2000). Contrary to Heinselman (2000), who assumed that the source of the SSL was sodium atoms, we propose that the major source may be sodium ions in a normal sodium layer. Furthermore, we will show the SSL was located in a lower-temperature region and there is no significant temperature enhancement inside the SSL. In Sect. 2, we will describe instruments and data sets utilized in this study. In Sect. 3, observational results will be presented. In Sect. 4, possible generation mechanisms are evaluated and then major mechanisms are proposed. This paper ends with a summary in Sect. 5.

2 Data sets and instruments

In this section, we briefly describe instruments used in this study. It should be pointed out that all the instruments were operated at the same observational field: Ramfjordmoen, Tromsø, Norway (69.6° N, 19.2° E), the so-called EISCAT Tromsø site.

2.1 The sodium lidar

The sodium temperature lidar (hereafter, sodium lidar) has a stable laser unit and five sets of telescopes (355 mm diameter Schmidt–Cassegrain) and receivers. The laser unit consists of an all-solid-state Q-switched single-frequency source tuned to the sodium D-2 line at 589.1583 nm. The source is based on sum frequency mixing two injection-locked Nd:YAG lasers in LiB_3O_5, which was used under 90° phase-matching conditions at a temperature of 40.7° on the night of 22 January 2012. Transmitted laser power was about 2.4 W. Photons returned from the sodium layer and collected by the receiving telescopes were integrated for 5 s with a 96 m range resolution. Five receivers were utilized for the night, and the five telescopes were pointed in a vertical direction. Under a two-frequency mode used to calculate a neutral temperature (cf. She et al., 1990; She and Yu, 1995), we changed the frequency every 1 min, so that we can derive temperature data with a 2 min temporal resolution. An optical filter with 1 nm bandwidth was employed with each receiver. More information on the sodium lidar system at Tromsø is described in Nozawa et al. (2014).

2.2 The EISCAT UHF radar

The EISCAT UHF radar (cf. Folkestad et al., 1983) was operated continually from about 07:40 UT on 13 January to 23:00 UT on 23 January 2012 with a scanning mode (so-called ip2) with three antenna positions. The antenna positions of azimuth and elevation were set to be (186, 70°), (0, 90°), and (98, 70°), and hereafter we call them position 1, position 2, and position 3, respectively. The sequence of the scanning was position 1, position 2, position 3, position 2, and back to position 1, and the dwell times were 95, 55, 95, and 55 s, respectively, i.e., the cycle time was 5 min. In other words, the three positions can be called south, vertical, and east positions, and the spatial separation between position 2 (vertical) and position 1 (south) or 3 (east) is about 36 km at 100 km altitude. The EISCAT UHF radar in this experiment (named "beata") transmitted two kinds of pulses: one alternating code and two power profiles. Data from the alternating code are used to derive ionospheric plasma parameters, such as ion and electron temperature. The power profile data enable us to derive an electron density profile assuming a fixed temperature ratio (i.e., $T_e / T_i =$ constant; T_e and T_i are electron and ion temperature, respectively). One of the power profile pulses covered an altitude range in a vertical position between 92.7 and 736.7 km with a 95.9 km altitude resolution, and the other covered an altitude range between 49.5 and 277.4 km with a 2.2 km altitude resolution. In this study, we used higher-resolution (i.e., 2.2 km) data. The transmit power was about 1.8 MW, and the electron density values were calibrated by using ionosonde data.

2.3 The photometer and the meteor radar

The photometer was pointed along the approximately local geomagnetic field line (azimuth: 182.6°; elevation: 77.5°) with a field of view of 1.2°. It was equipped with three optical filters tuned for wavelengths of 427.8, 557.7, 630.0 nm with FWHMs of 2, 3, and 2 nm, respectively. The photometer receives photons through the three filters simultaneously, at a sampling rate of 20 Hz.

The meteor radar (MR) at Tromsø (Hall et al., 2005) installed in 2003 can continually provide neutral wind velocity data, together with a meteor count with a 2 km altitude and 1 h time resolution in the height range from approximately 80 to 100 km. This radar system operates at 30.25 MHz. The field of view of this MR is about 140°: a spatial averaging over perhaps 200 km at the peak echo occurrence height. Descriptions of the determination of wind velocity may be

found, for example, in works by Aso et al. (1979) and Tsutsumi et al. (1999).

3 Observational results

In this section, we describe observational results obtained by the sodium lidar, the EISCAT UHF radar (vertical position), and the photometer. Since the photometer was pointed at the field-aligned position, the volume of the photometer observation was about 22 km southward from the vertical observation at an altitude of 100 km. Figure 1a and b show temporal and altitude variations in the sodium density and the neutral temperature, respectively, from 16:00 UT on 22 January to 04:00 UT on 23 January 2012, obtained by the sodium lidar. The sodium density and the neutral temperature were derived with a 2 min temporal and about a 0.5 km altitude resolution (smoothing in altitude with Hanning window). From Fig. 1a, we can identify a peculiar region with higher sodium density at 93–94 km between 21:18 and 21:36 UT above a normal sodium layer located at about 80–90 km. After 21:40 UT there is a thinner sodium density layer at around 95–97 km, which gradually descends to about 90 km by 24:00 UT. These higher sodium density regions are thought to be so-called SSLs, and we mainly focus on generation mechanisms of the SSL appearing at 93–94 km in this paper.

From Fig. 1b, below 90 km, the neutral temperature varied from about 210 to 260 K. There seemed to be a lower-temperature region around 92–98 km between 20:00 and 22:00 UT, indicating that the SSL appeared in the lower-temperature region. This lower-temperature region would result mainly from a semidiurnal tidal variation. Due to quick temporal and large altitudinal variations in the sodium density, the temperature values around and inside the SSL region could be unreliable, and we have derived the values with higher temporal resolution and present the results later in this session.

Figure 1c, d, and e show temporal and altitude variations in the electron density and emission intensities at 427.8 and 557.7 nm obtained by the EISCAT UHF radar in the vertical position and the photometer with the field-aligned position, respectively. The photometer measurements clearly showed that auroral particle precipitation intermittently occurred throughout the night, and the electron density profile indicated that the auroral particle precipitation often reached 95 km and below, indicating frequent precipitation of high-energy (greater than 30 keV) particles (cf. Rees, 1963).

In addition to the auroral ionizations, there are two layered structures associated with a relatively high electron density of over $10^{10}\,m^{-3}$ appearing between 20:00 and 24:00 UT. Although auroral ionization contaminated their identification, the upper layer appeared at about 105 km at 20:00 UT, gradually descended, and stayed at around 94 km between 21:18 and 21:40 UT, ascended and reached about 97 km at 21:50 UT, and again descended to 88 km afterwards. The

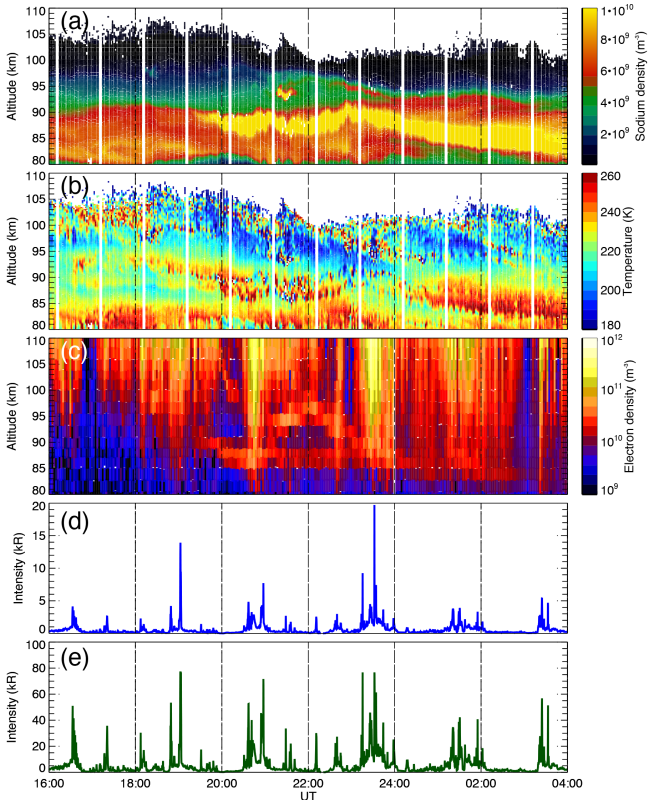

Figure 1. Variations in the sodium density **(a)**, the neutral temperature **(b)**, and the electron density **(c)**; the emission intensity (10 s averaged values) of 427.8 nm **(d)** and 557.7 nm **(e)** from 16:00 UT on 22 January to 04:00 UT on 23 January are shown. The temporal and altitude resolution in **(a)** and **(b)** is 2 min and 0.5 km, and it is 30 s and about 2.2 km in **(c)**.

lower layer appeared at 90 km at 19:30 UT and descended and reached at 87 km at 20:00 UT and stayed there until 24:00 UT. These layers were likely sporadic E (Es) layers consisting of metal ions (Fe^+, Ca^+, Na^+, etc.) and electrons.

Figure 2a shows variations in the sodium density as well as the altitude of the maximum sodium density from 20:00 to 24:00 UT between 90 and 100 km with a 2 min and a 0.5 km resolution (smoothing in altitude with Hanning window). Figure 2b and c present temporal variations in the maximum sodium density of the SSL and the ratio of the maximum sodium density to the background normal sodium density at the same altitude, respectively. The background normal sodium density is the averaged value between 16:00 and 19:00 UT at each altitude when the sodium density varied smoothly with time. The ratio rapidly increased from 1.9 to 5.8 for 2 min from 21:16 to 21:18 UT. In this study, the SSL was defined by stating that the ratio of the maximum density to the background normal density is greater than 2 (cf. Simonich, 2005).

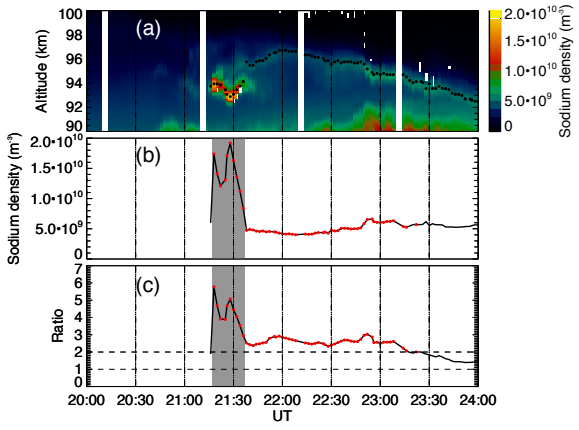

Figure 2. (a) Variations in the sodium density from 20:00 to 24:00 UT on 22 January 2012 between 90 and 100 km are presented. Black dots denote altitudes of the maximum density of the SSL(s). **(b)** The maximum sodium density of the SSL(s). **(c)** The ratio of the maximum sodium density to the background sodium density at the same altitude. Red dots in **(b)** and **(c)** denote data values with a ratio greater than 2. In this study, we mainly focus on the SSL occurring for time intervals shown in the gray shade (i.e., 21:18 and 21:36 UT).

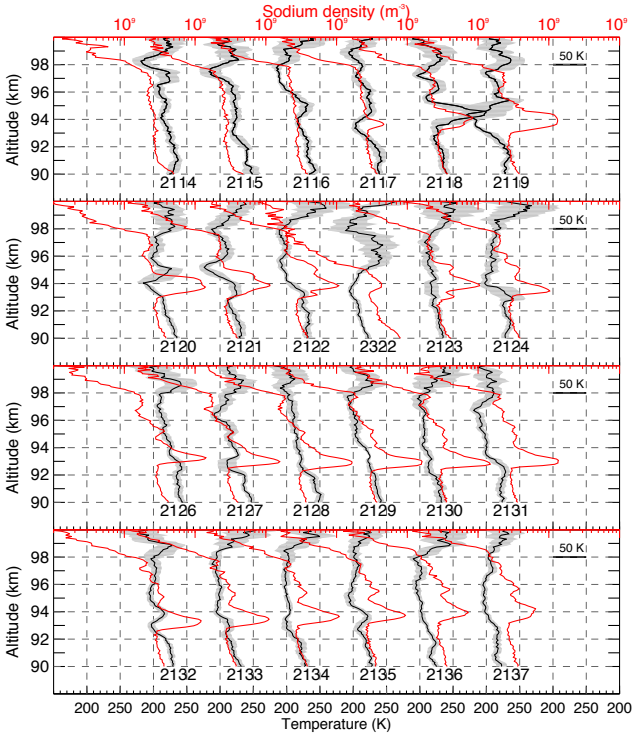

Figure 3. Altitude profiles of sodium density (red line) and neutral temperature (black line) from 21:14 to 21:37 UT every 1 min on 22 January 2012 are presented. These values are derived with a 15 s temporal and 96 m height resolution. A 1 km running average is applied to the temperature profile. The gray shade shows standard deviations of the temperature data (1σ).

The maximum altitude of the SSL changed by 1 km to about 93 km at 21:28 UT when the sodium density maximized, and rose by 1 km to about 94 km from 21:30 to 21:36 UT. At around 21:38 UT, another SSL appeared at around 97 km. After 22:00 UT, the maximum altitude of the SSL gradually fell and reached about 92 km at 24:00 UT. The sodium density inside the first SSL rapidly increased from $\sim 6.0 \times 10^9$ to $\sim 1.7 \times 10^{10}\,\mathrm{m}^{-3}$ in 2 min between 21:16 and 21:18 UT. After the first sudden enhancement, the sodium density inside the SSL decreased to $1.2 \times 10^{10}\,\mathrm{m}^{-3}$ at 21:22 UT and again increased to $\sim 1.9 \times 10^{10}\,\mathrm{m}^{-3}$ at 21:28 UT. From 21:28 to 21:36 UT, the sodium density of the SSL gradually decreased from 1.9×10^{10} to $8.0 \times 10^9\,\mathrm{m}^{-3}$; at 21:38 UT the ratio of the maximum sodium density to the background sodium density became lower than 2. The FWHM of the SSL at 21:28 UT was ~ 1.1 km. At 21:38 UT, another SSL appeared at 97 km. The maximum sodium density of the later SSL was lower than that of the earlier one, but between 21:40 and 23:00 UT the maximum sodium density was still a few times higher than that of the background.

The sodium density inside the SSL observed from 21:18 to 21:36 UT drastically changed with time and altitude; thus, the derivation of the temperature requires a high spatial and temporal resolution. The sodium lidar at Tromsø recorded signals every 5 s and switched the frequencies every 1 min. Since data obtained during the frequency-switching interval have to be removed due to a possible mixing of the two types of frequency data, we have derived the temperature with 15 s temporal and 96 m altitude resolution every 1 min.

Figure 3 compares the altitude profile of the sodium density and the neutral temperature derived with a 15 s temporal and 96 m altitude resolution. For temperature data, 1 km running averaged values are presented every 96 m with a 15 s temporal resolution. The enhancement of the sodium density began at 21:17 UT around 94 km. The maximum density altitude was located at the local temperature minimum at 21:17, 21:19, and 21:20 UT in contrast to Gardner et al. (1993), who pointed out that the SSL was located in the higher-temperature region. Although at times the temperature increased inside or nearby the SSL, no trend of temperature can be seen inside the SSL. Considering possible variations in temperature due to atmospheric waves, we can conclude that the SSL in this event was not located in an enhanced temperature region.

4 Discussion

Much attention has been paid to the generation mechanisms of SSLs for about 35 years since Clemesha et al. (1978) first reported an SSL. Possible proposed candidates are the supply of sodium atoms from an Es layer, an effect of the electric field (downward ion motion), chemical reactions due to

local temperature enhancements, meteor absorption, and auroral particle sputtering (cf. Kane et al., 1993; Heinselman, 2000; Kirkwood and von Zahn, 1991; Gardner et al., 1993; Clemesha et al., 1988; von Zahn and Hansen, 1988). The key requirements for any mechanism to fulfill are how to supply enhanced sodium atoms and how to make a thin layer structure with a large horizontal extent. Supply of sodium atoms from an Es layer has been considered the most possible generation mechanism. Kane et al. (1993) argued that an Es layer triggered the release of sodium atoms, but the Es layer was not the major source of the SSL observed at Arecibo. This is because the number of sodium ions contained in the Es layer was not enough for the generation of the SSL compared to IS radar and lidar observations.

4.1 Production from the Es layer

As shown in Fig. 1c, the two Es layers appeared between 80 and 110 km between approximately 20:00 and 24:00 UT on 22 January 2012. Figure 4a compares maximum density altitudes of the SSL and the upper Es layer. When the SSL appeared at 21:18 UT, the SSL was located at almost the same altitude of the upper Es layer (observed in the vertical direction (position 2) of the EISCAT UHF radar). The maximum altitude of the SSL descended and then ascended between about 93 and 94 km between 21:18 and 21:36 UT, while the Es layer remained at 94 km. During the time interval, the difference in the altitudes between the Es layer and the SSL was about 1 km at most. Thus we can propose that the SSL and the Es layer were located at the same altitude considering the lower altitude resolution (2.2 km) of the EISCAT measurements. This implies that the Es layer contributed to the generation of the SSL (to some extent). Furthermore, the Es layer was observed at almost the same altitude as three positions of the EISCAT measurements, suggesting the Es layer and (probably) the SSL extended at least 36 km in a horizontal direction. Figure 4c shows the ratio of the sodium density (red: 0.5 km resolution; blue: 2.2 km resolution) to the electron density. The ratio with the 0.5 km (2.2 km) resolution data varied from 0.56 (0.31) to 0.27 (0.16) between 21:18 and 21:30 UT. Figure 4d shows column densities integrated between 92 and 97 km of the electron densities and sodium densities. An increase in the sodium column density requires source(s) of sodium atoms (cf. Simonich, 2005).

The conversion of sodium ions in an Es layer to sodium atoms through a charge exchange process or clustering reactions has been discussed as a major source of high-density SSLs appearing between 90 and 100 km (von Zahn and Hansen, 1988). Some in situ measurements suggest that sodium ion abundance is several percent of the total abundance. Kane et al. (1993) estimated that the sodium ion abundance in an Es layer was 10 % at most. Figure 4b shows variations in sodium and electron densities. The red and blue lines show variations in the peak sodium densities of the SSL with altitude resolutions of 0.5 and 2.2 km, respectively. The averaged maximum electron density from 20:00 to 21:18 UT was 3.0×10^{10} m^{-3}, with a standard deviation of 1.3×10^{10} m^{-3}. The averaged maximum sodium densities of the SSL with an altitude resolution of 0.5 and 2.2 km from 21:18 to 21:36 UT were 1.4×10^{10} and 8.2×10^{9} m^{-3}, with standard deviations of 3.3×10^{9} and 1.7×10^{9} m^{-3}, respectively. When we assume that the Es layer contained sodium ions numbering 10 % of the total (cf. Hansen and von Zahn, 1990; Kane et al., 1993; Heinselman, 2000), the amount of the sodium ions was 3.0×10^{9} m^{-3}, which corresponds to about 21 % for the 0.5 km resolution data and to about 37 %

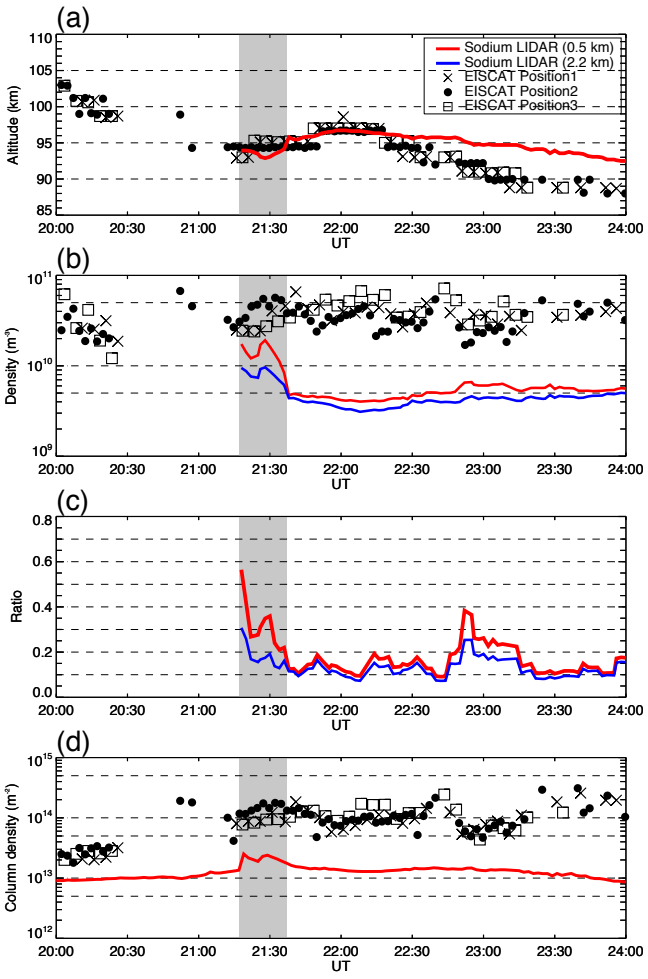

Figure 4. (a) Variations in altitudes of the maximum SSL (red line) and the Es layer for three different directions (square, closed circle, and triangle) of the EISCAT UHF radar measurements are compared. Shaded area denotes the time interval when the SSL was seen. **(b)** Same as **(a)** except for the density with 0.5 km (red line) and 2.2 km (blue line) altitude resolution. **(c)** Variations in the ratio of the maximum sodium density of the SSL with 0.5 km (red line) and 2.2 km (blue line) altitude resolution to the maximum electron density in the Es layer (in the vertical position of the EISCAT measurements) are shown. **(d)** Comparison of column densities integrated between 92 and 97 km are shown.

for the 2.2 km resolution data of the averaged maximum sodium density of the SSL. Furthermore, even if we assume the abundance of sodium ions to be 20 % in the Es layer, the amount of sodium ions corresponds to less than 74 %. These results indicate that the Es layer alone could not provide enough of a supply of sodium atoms in this event but probably contributed to their generation to some extent.

4.2 Concentration from a sodium ion layer through electric field

Kirkwood and von Zahn (1991) proposed a possibility for concentration of metallic ions through electric fields. Plane (2004) proposed that Na^+ distributes around the topside of a sodium layer as a reservoir of the sodium layer, and its shape is the Gaussian distribution with an altitude of maximum density of about 105 km. We evaluate the effects of the electric field for Na^+. A normal sodium ion layer usually exists under equilibrium conditions with a sodium layer (cf. Plane, 2004). On the other hand, the source of an Es layer would be somewhat different: a sufficient abundance of metallic ions is required (cf. Bedey and Watkins, 1997, 1998). Bedey and Watkins (1997) proposed large-scale transport of metallic ions in the polar ionosphere as the source of an Es layer. Here, we assume that the Es layer coexisted with the normal sodium ion layer.

Figure 5 shows the direction and the strength of the electric field derived by the EISCAT UHF radar data with a 10 min resolution from 18:00 to 24:00 UT on 22 January 2012. Before 20:00 UT, the direction of the electric field fluctuated between the north, west, and south with a strength of 25 mV m^{-1} or less. From 20:20 to 21:30 UT, the direction gradually changed from the south through the west to the northwest with an intensity of 17–45 mV m^{-1}. The southwestward electric field works most effectively for the downward motion of charged particles below 120 km (Bedey and Watkins, 2001; Oyama et al., 2012). From 21:30 to 22:40 UT, the direction of the electric field changed from the northwest to the south with an intensity of 10–60 mV m^{-1}, and from 22:40 to 24:00 UT the direction was approximately southward.

To evaluate the effects of the electric field, we have calculated its contributions based on a continuity equation in the vertical direction:

$$\frac{\mathrm{d}n_{\mathrm{si}}(z)}{\mathrm{d}t} = q_{\mathrm{si}}(z) - L_{\mathrm{si}}(z) - \frac{\mathrm{d}}{\mathrm{d}z}\left(n_{\mathrm{si}}(z)v_{\mathrm{si}}(z)\right), \quad (1)$$

where $n_{\mathrm{si}}(z)$ is sodium ion density at height z, $q_{\mathrm{si}}(z)$ is the sodium ion production rate, $L_{\mathrm{si}}(z)$ is the sodium ion loss rate, and $v_{\mathrm{si}}(z)$ is the vertical sodium ion velocity and is counted positively upwards. The vertical sodium ion velocity is expressed as follows (cf. Kirkwood and von Zahn, 1991):

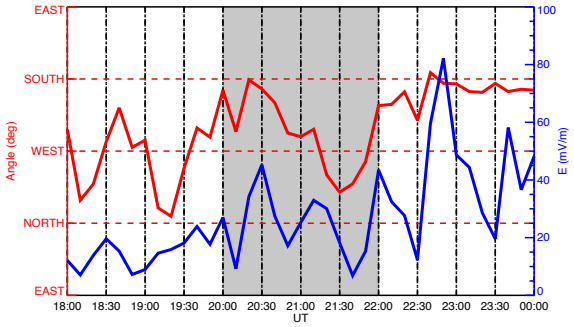

Figure 5. Temporal variations in the direction (red line) and the strength (blue line) of the electric field derived by the EISCAT UHF radar from 18:00 to 24:00 UT on 22 January 2012 are shown.

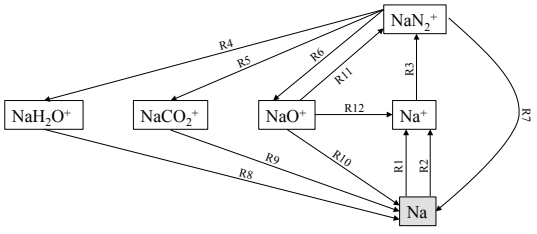

Figure 6. Schematic drawing of circular reactions among Na, Na^+, NaN_2^+, NaO^+, NaH_2O^+, NaH_2O^+, and $NaCO_2^+$.

$$v_{\mathrm{si}}(z) = \frac{\Omega_{\mathrm{si}}\nu_{\mathrm{in}}(z)}{\Omega_{\mathrm{si}}^2 + \nu_{\mathrm{si}}^2}\left(\frac{E_{\mathrm{N}}}{B_0}\sin I + W_{\mathrm{E}}(z)\right)\cos I + \frac{\Omega_{\mathrm{si}}^2}{\Omega_{\mathrm{si}}^2 + \nu_{\mathrm{si}}^2(z)}\left(\frac{E_{\mathrm{E}}}{B_0} - W_{\mathrm{N}}(z)\sin I\right)\cos I + \left(1 - \frac{\cos^2 I\,\Omega_{\mathrm{si}}^2}{\Omega_{\mathrm{si}}^2 + \nu_{\mathrm{in}}^2(z)}\right)W_Z(z), \quad (2)$$

where Ωs_i is sodium ion gyro frequency, ν_{in} is ion neutral collision frequency (given by Eq. (2.29a) in Kelley, 2009), I is the inclination of the earth's magnetic field obtained with IGRF geomagnetic model ($I = 78.1°$ at Tromsø at 100 km), E_{N} and E_{E} are the northward and eastward components of the electric field, $W_{\mathrm{N}}(z)$, $W_{\mathrm{E}}(z)$, and $W_z(z)$ are the northward, eastward, and upward components of the neutral wind, and B_0 is the strength of the earth's magnetic field. Kirkwood and von Zahn (1991) simulated Fe^+ development based on the continuity equation, but they used the continuity equation without the ion production and the ion loss rate. Because related chemical reactions cannot be negligible below about 100 km, the ion production and the loss rate in the continuity equation are included in this study.

Chemical reaction processes for sodium atoms and ions in a sodium layer are complicated. For simplification, we consider the circular reactions as shown in Fig. 6. The processes

consist of the following reactions (Plane, 2004):

$$\mathrm{Na} + \mathrm{O_2}^+ \rightarrow \mathrm{Na}^+ + \mathrm{O_2}$$
$$: k_{20} = 2.7 \times 10^{-15}\ (\mathrm{m^3\,s^{-1}}) \quad \text{(R1)}$$

$$\mathrm{Na} + \mathrm{NO}^+ \rightarrow \mathrm{Na}^+ + \mathrm{NO}$$
$$: k_{21} = 8.0 \times 10^{-16}\ (\mathrm{m^3\,s^{-1}}) \quad \text{(R2)}$$

$$\mathrm{Na}^+ + \mathrm{N_2} + \mathrm{N_2} \rightarrow \mathrm{NaN_2}^+ + \mathrm{N_2}$$
$$: k_{22} = 4.8 \times 10^{-42}(T/200)^{-2.2}\ (\mathrm{m^6\,s^{-1}}) \quad \text{(R3)}$$

$$\mathrm{NaN_2}^+ + \mathrm{H_2O} \rightarrow \mathrm{NaH_2O}^+ + \mathrm{N_2}$$
$$: k_{24} = 6 \times 10^{-16}\ (\mathrm{m^3\,s^{-1}}) \quad \text{(R4)}$$

$$\mathrm{NaN_2}^+ + \mathrm{CO_2} \rightarrow \mathrm{NaCO_2}^+ + \mathrm{N_2}$$
$$: k_{24} = 6 \times 10^{-16}\ (\mathrm{m^3\,s^{-1}}) \quad \text{(R5)}$$

$$\mathrm{NaN_2}^+ + \mathrm{O} \rightarrow \mathrm{NaO}^+ + \mathrm{N_2}$$
$$: k_{25} = 4 \times 10^{-16}(\mathrm{m^3\,s^{-1}}) \quad \text{(R6)}$$

$$\mathrm{NaN_2}^+ + e^- \rightarrow \mathrm{Na} + \mathrm{N_2}$$
$$: k_{29} = 1 \times 10^{-12}(T/200)^{-0.5}\ (\mathrm{m^3\,s^{-1}}) \quad \text{(R7)}$$

$$\mathrm{NaH_2O}^+ + e^- \rightarrow \mathrm{Na} + \mathrm{H_2O}$$
$$: k_{29} = 1 \times 10^{-12}(T/200)^{-0.5}\ (\mathrm{m^3\,s^{-1}}) \quad \text{(R8)}$$

$$\mathrm{NaCO_2}^+ + e^- \rightarrow \mathrm{Na} + \mathrm{CO_2}$$
$$: k_{29} = 1 \times 10^{-12}(T/200)^{-0.5}\ (\mathrm{m^3\,s^{-1}}) \quad \text{(R9)}$$

$$\mathrm{NaO}^+ + e^- \rightarrow \mathrm{Na} + \mathrm{O}$$
$$: k_{29} = 1 \times 10^{-12}(T/200)^{-0.5}\ (\mathrm{m^3\,s^{-1}}) \quad \text{(R10)}$$

$$\mathrm{NaO}^+ + \mathrm{N_2} \rightarrow \mathrm{NaN_2}^+ + \mathrm{O}$$
$$: k_{27} = 1 \times 10^{-18}\ (\mathrm{m^3\,s^{-1}}) \quad \text{(R11)}$$

$$\mathrm{NaO}^+ + \mathrm{O} \rightarrow \mathrm{Na}^+ + \mathrm{O_2}$$
$$: k_{26} = 1 \times 10^{-17}\ (\mathrm{m^3\,s^{-1}}), \quad \text{(R12)}$$

where T is the temperature. In this study, we calculate the density developments of sodium atoms, sodium ions, $\mathrm{NaN_2}^+$, $\mathrm{NaCO_2}^+$, $\mathrm{NaH_2O}^+$ and NaO^+ by numerical analysis of the following equations:

$$\frac{\mathrm{d[Na]}}{\mathrm{d}t} = k_{29}[\mathrm{NaN_2}^+][e^-] + k_{29}[\mathrm{NaO}^+][e^-] + k_{29}[\mathrm{NaCO_2}^+][e^-] + k_{29}[\mathrm{NaH_2O}^+][e^-] - k_{20}[\mathrm{Na}][\mathrm{O_2}^+] - k_{21}[\mathrm{Na}][\mathrm{NO}^+] \quad (3)$$

$$\frac{\mathrm{d[Na}^+]}{\mathrm{d}t} = k_{20}[\mathrm{Na}][\mathrm{O_2}^+] + k_{21}[\mathrm{Na}][\mathrm{NO}^+] + k_{26}[\mathrm{NaO}^+][\mathrm{O}] - k_{22}[\mathrm{Na}^+][\mathrm{N_2}][\mathrm{N_2}] \quad (4)$$

$$\frac{\mathrm{d[NaN_2}^+]}{\mathrm{d}t} = k_{22}[\mathrm{Na}^+][\mathrm{N_2}][\mathrm{N_2}] + k_{27}[\mathrm{NaO}^+][\mathrm{N_2}] - k_{29}[\mathrm{NaN_2}^+][e^-] - k_{25}[\mathrm{NaN_2}^+][\mathrm{O}] - k_{24}[\mathrm{NaN_2}^+][\mathrm{CO_2}] - k_{24}[\mathrm{NaN_2}^+][\mathrm{H_2O}] \quad (5)$$

$$\frac{\mathrm{d[NaO}^+]}{\mathrm{d}t} = k_{25}[\mathrm{NaN_2}^+][\mathrm{O}] - k_{26}[\mathrm{NaO}^+][\mathrm{O}] - k_{27}[\mathrm{NaO}^+][\mathrm{N_2}] - k_{29}[\mathrm{NaO}^+][e^-] \quad (6)$$

$$\frac{\mathrm{d[NaCO_2}^+]}{\mathrm{d}t} = k_{24}[\mathrm{NaN_2}^+][\mathrm{CO_2}] - k_{29}[\mathrm{NaCO_2}^+][e^-] \quad (7)$$

$$\frac{\mathrm{d[NaH_2O}^+]}{\mathrm{d}t} = k_{24}[\mathrm{NaN_2}^+][\mathrm{H_2O}] - k_{29}[\mathrm{NaH_2O}^+][e^-]. \quad (8)$$

The initial condition of an altitude profile of sodium atoms is given by the averaged profile between 16:00 and 19:00 UT. For Na^+, a Gaussian distribution is assumed with a maximum altitude of 105 km, an FWHM of 10 km, and a peak density of $3.5 \times 10^9\ \mathrm{m^{-3}}$ after Plane (2004). Additional sodium ions from the Es layer are included: the amount is 10 % of the electron density at 104 km. The initial condition for $\mathrm{NaCO_2}^+$ is assumed with 1 / 10 of the density of Na^+ at 20:00 UT. The initial condition of densities of $\mathrm{NaN_2}^+$, $\mathrm{NaH_2O}^+$, and NaO^+ are assumed to be 0. We assumed the molecular ion abundance (e.g., 77 % NO^+ and 17 % $\mathrm{O_2}^+$ at 94 km) of the total electron density (obtained by the EISCAT UHF radar measurements) with reference to the IRI (International Reference Ionosphere) model (Bilitza, 2001) outside the Es layer (in particular, during auroral particle precipitation intervals (e.g., around 20:57 UT)), while 10 % (NO^+) and 1 % ($\mathrm{O_2}^+$) were assumed in the Es layer: the latter assumption values are somewhat arbitrary. It should be pointed out that the molecular ions (NO^+ and $\mathrm{O_2}^+$) work on the loss of sodium atoms through Reactions (R1) and (R2). The neutral densities of major species (e.g., $\mathrm{N_2}$, $\mathrm{O_2}$, O) are given by mass spectrometer incoherent scatter (MSIS-E-90) Atmosphere Model (Hedin, 1991). The densities of $\mathrm{CO_2}$ and $\mathrm{H_2O}$ are given as follows (Allen, 1963):

$$[\mathrm{CO_2}] = (3 \times 10^{-4}/0.7811)[\mathrm{N_2}] \quad (9)$$

$$[\mathrm{H_2O}] = (5 \times 10^{-7}/0.7811)[\mathrm{N_2}]. \quad (10)$$

The calculation started at 20:00 UT. The number density of each species was calculated with a time step of 1 min and vertical resolution of 0.1 km between 80 and 120 km until 22:00 UT.

Figure 7a and b illustrate temporal variations in the density profiles of sodium ions and sodium atoms, respectively. In this calculation, the electric field values, horizontal wind velocity values (above 100 km), and the electron density values

are given from the EISCAT radar measurements; horizontal wind velocities at and below 100 km are given from MR data. Neutral temperature values at and below 100 km are given by the sodium lidar measurements, while above 100 km, they are given by the MSIS-E-90 Atmosphere Model. The vertical wind velocity was assumed to be 0 over the height region.

We briefly summarize the development of layers of sodium ions and sodium atoms. Sodium ions in the normal sodium ion layer were transported downward by the electric field. The vertical profile of the sodium ion layer becomes significantly thinner because collisional coupling with the neutral atmosphere significantly increases with decreasing altitude, causing the sodium ions to "pile up" as the calculation progresses (cf. Bedey and Watkins, 1997). Thus, a thin dense layer of the sodium ions forms around 94 km. Since the molecular nitrogen density around 94 km is high, sodium ions were swiftly converted to NaN_2^+ due to the Reaction (R3). In this event, the Es layer was located at approximately the same altitude as the SSL. The NaN_2^+ were likely neutralized with the electrons in the Es layer, and then sodium atoms were produced around 94 km with a thickness of about 2 km. An SSL was generated through these processes with the loss processes of Reactions (R1) and (R2). The densities of molecular ions (NO^+ and O_2^+), which contribute to loss of the sodium atoms, are very low around 94 km when no auroral particle precipitation occurs. In addition, we neglect the diffusion effect in this calculation. Therefore, the generated SSL can last for 30 min or longer in this calculation.

Figure 7a shows a temporal development of the redistribution of sodium ions. At 21:18 UT, the altitude of maximum sodium ions reached 94.2 km, and the maximum sodium ion density decreased with time after 20:45 UT, indicating the chemical recombination of sodium ions to sodium atoms. Since N_2 density increases exponentially with decreasing altitude, the conversion of sodium ions to sodium atoms enhances with decreasing altitude. Furthermore, the altitude of the maximum sodium ion density ascended from 21:20 to 21:40 UT by about 2 km.

Figure 7b shows that the calculation suitably produced a thin layer with high sodium density and with an FWHM of about 2 km. The sodium density steadily increased from 21:10 to 21:40 UT. The sodium density was enhanced from 2.4×10^9 m^{-3} at 20:00 UT to 1.5×10^{10} m^{-3} at 21:18 UT at 94.4 km. The value at 21:18 UT corresponds to about 88 % of the observed value at 94 km, and at 21:28 UT the calculated density of the sodium atom was 1.7×10^{10} m^{-3}, which was about 89 % of the observed value. The calculation shows that the maximum sodium density reached 1.9×10^{10} m^{-3} at 21:40 UT, which was about the same as the observed maximum sodium density at 21:28 UT. Although the calculation, which mainly used observational values, did not completely reproduce the observational results, some important features (e.g., a thin layer, a maximum sodium density altitude, and an enhanced sodium density) were well produced. Therefore, we propose that (1) the major source was sodium ions in a normal sodium ion layer and (2) the electric field played a major role in generating the SSL in this event.

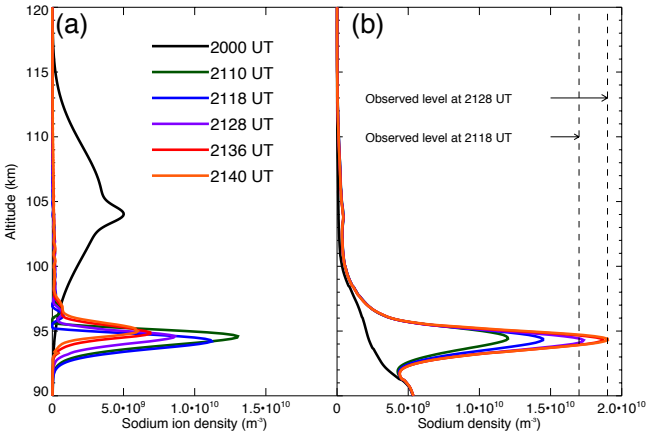

Figure 7. Temporal developments of sodium ions **(a)** and sodium atoms **(b)** are illustrated.

4.3 Effect of temperature

Figure 8 compares sodium column density and mean neutral temperature between 92 and 97 km derived with a 15 s temporal and 96 m altitude resolution. The mean temperature decreased from 18:00 to 20:45 UT, while the sodium column density gradually increased. The mean temperature increased from 20:45 to 21:00 UT and decreased again from 21:00 to 22:00 UT. After about 22:00 UT, the mean temperature increased and the sodium column density tended to decrease. The background temperature between 20:30 and 23:30 UT was lower by about 20 K than that for the other intervals. Thus, there was a tendency for the background temperature to be in inverse proportion to sodium column density. Since the sodium production is in inverse proportion to the background neutral temperature Reactions (R7, R8, R9, R10), the background temperature condition seemed to support the generation of the SSL in this event. The calculation also supports the idea that when the temperature was set to be constant (230 K), the calculated maximum sodium density was reduced by about 6 % from the value of the calculation using the real temperature conditions.

4.4 Meteor absorption and auroral particle sputtering

Figure 9 shows variations in the meteor count observed by MR at Tromsø from 12:00 to 24:00 UT on 22 January 2012. Monthly averaged values for January 2012 are also illustrated for comparison. Figure 9 shows no remarkable increase in the meteor count between 12:00 and 24:00 UT, not even around 21:00 UT on 22 January 2012. Moreover, the temporal variation in the meteor count for 22 January is similar to that of the monthly average, but the number of counts was lower

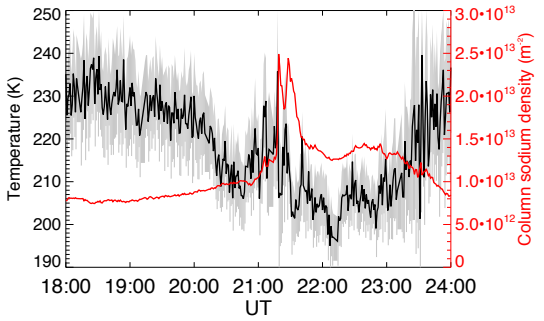

Figure 8. Comparison of sodium column density (red line) and mean temperature (black line) between 92 and 97 km every 1 min. The sodium density and the temperature are derived with a 15 s temporal and 96 m height resolution. The gray shading denotes standard deviations from the mean temperature.

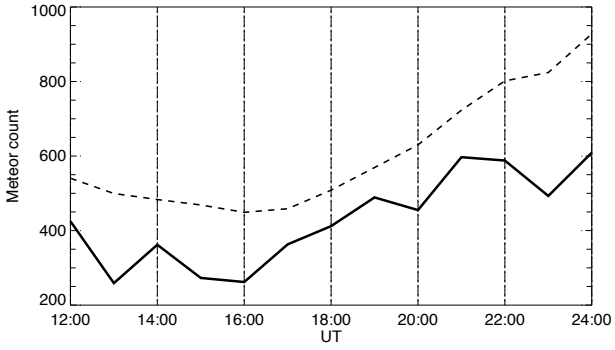

Figure 9. Variations in meteor count from 12:00 to 24:00 UT on 22 January 2012 observed by the meteor radar at Tromsø are shown by the solid line. Dashed line denotes monthly averaged meteor counts in January 2012.

than the monthly averaged values. These results imply that the meteor shower did not occur during this time interval. If a cosmic bombardment with a mass of over 100 kg comes into the atmosphere, it must be detected as a bright trail by an all-sky digital camera. Such a bright trail was not seen in images operated at the same observational field. Therefore, we can exclude the possibility of the effect of meteors and/or meteor showers.

According to von Zahn and Hansen (1988), auroral particles with an energy higher 40 keV may provide sodium atoms from dust particles. Figure 1c shows that the electron density was enhanced below 90 km at 20:57 UT due to auroral particle precipitation. In this time interval, the auroral particles, which penetrated into 90 km or lower, should have an energy of 40 keV or higher (cf. Rees, 1963; Heinselman, 2000). Although the sodium atoms are sputtered quickly from dust particles through the auroral sputtering process (von Zahn and Hansen, 1988), the auroral particle precipitation occurred about 20 min earlier than the time of the commencement of the SSL generation. Therefore, the auroral particle sputtering is unlikely to be a major contributor to the SSL generation. On the other hand, since the auroral activity was high over the night, the aurora particle precipitation might have produced additional sodium ions through the charge exchange process (cf. Heinselman, 2000); consequently, the background density of sodium ions might be increased. For example, a life time of a sodium ion at 93 km is about 30 min (Cox and Plane, 1998). Through this process, there would be the possibility that the auroral particle precipitation (as another source) contributed to the generation of the SSL to some extent.

4.5 The effect of advection

For generation mechanisms of SSLs, such a rapid increase in the sodium density implies a possibility of advection (cf. Clemesha et al., 1978; Batista et al., 1991). Since the sodium lidar observed only the vertical direction on the night of 22 January 2012, the evaluation of the effect of the advection is rather difficult. As we mentioned, the Es layer extended at least 36 km southward and eastward from the vertical position at Tromsø. As the SSL advent and the Es layer occur at the same time, we could assume the SSL would have also a similar extent to the Es layer. The lifetime of the SSL (about 18 min) and the eastward wind (30 m s^{-1}) might suggest the advection effect and explain the rapid increase in the sodium density, since the movement value ($= 18\,\text{min} \times 30\,\text{m s}^{-1}$) is about 32 km, similar to the extent (about 36 km). Even if the rapid increase in the sodium density from 21:16 to 21:18 UT was due to the advection, we could say that the SSL was generated nearby the field of view of the sodium lidar. This is because, as already mentioned before, the EISCAT radar and MR observational values, used in the calculation of the temporal development of the normal sodium ion layer, are spatial averages to some extent.

At any rate, by using the point measurement data of the sodium lidar, we cannot exclude the possibility of (horizontal) advection. We have made five beam observations (north, south, east, west, and vertical positions) with the sodium lidar at Tromsø since October 2012. Thus, we will carry out further investigations of the generation mechanisms of SSLs at high latitudes including the advection effect in the near future.

5 Conclusions

On 22 January 2012, an SSL was observed at about 93–94 km by the sodium lidar operated at a high-latitude station at Ramfjordmoen, Tromsø, Norway. The auroral activity was high for the night. From 21:18 to 21:36 UT, the sodium density inside the SSL was about 2 to 6 times greater than the background sodium density. The EISCAT UHF radar detected an Es layer above 90 km between about 20:00 and 23:00 UT. The Es layer was located at an altitude of about 94 km, where the SSL was observed from 21:18 to 21:36 UT.

This result is likely to indicate that the Es layer contributed to the SSL generation. The Es layer, however, could provide less than 37 % (at most) of the sodium atoms of the SSL if the abundance of sodium ions was 10 % and all the sodium ions were transported.

By using observational values obtained with multiple instruments and some model values, we have calculated a temporal development of sodium ions in a normal sodium ion layer considering chemical reactions and the effect of the electric field and the wind. In this calculation, we used observational data of the electric field, the horizontal wind velocity, neutral temperature (below 100 km), and the electron density. As the result of this calculation, those processes can provide about 88 % of the sodium atoms of the SSL at 94.4 km. No enhancement of the meteor count or a bright trail were observed, and auroral particle precipitation with high energy (40 keV or so) occurred 20 min earlier than the time of the commencement of the SSL generation. Thus, the effects of meteor absorption and auroral particle sputtering appear not to be dominant mechanisms in this event. Therefore, we have concluded that the major source was sodium ions in a normal sodium ion layer, and the SSL was generated by the conversion of sodium ions into sodium atoms by a combination of the following effects: (1) the redistribution of the sodium ions of a normal sodium ion layer due to the electric field with a strength of about 17–45 $\mathrm{mV\,m^{-1}}$ and (2) the higher electron density of the sporadic E-layer, which facilitated the chemical reactions, and also the Es layer supplying additional sodium ions. It should be pointed out that we have, mainly based on observational data, for the first time, demonstrated the possibility of sodium ions in a normal sodium ion layer as a (major) source of an SSL. Furthermore, we have shown that the SSL was located in the lower-temperature region and that there was no temperature enhancement inside the SSL in this event. More efforts are needed to elucidate the mechanisms of the rapid growth of the sodium atom density as well as the effect of advection.

Acknowledgements. The Tromsø sodium lidar project is mainly supported by Special Funds for Education and Research (Energy Transport Processes in Geospace) from the Ministry of Education, Culture, Sports, Science, and Technology in Japan (MEXT), in collaboration with Nagoya University, Shinshu University, RIKEN, The Arctic University of Tromsø, and the EISCAT Scientific Association. We are indebted to the director and staff of EISCAT for operating the facility and supplying the data. EISCAT is an International Association supported by China (CRIRP), Finland (SA), the Federal Republic of Germany (DFG), Japan (STEL and NIPR), Norway (NFR), Sweden (VR), and the United Kingdom (PPARC). We also acknowledge the use of geomagnetic data from the World Data Centers for Geomagnetism in Kyoto, Japan, and Copenhagen, Denmark, and the Kp indices from GeoForschungsZentrum Potsdam (http://www.gfz-potsdam.de). T. Takahashi is supported as a research fellow of the Japan Society for the Promotion of Science (JSPS) for Young Scientists. This research has been partly supported by MEXT through a Grant-in-Aid for JSPS fellows (25-3733), Scientific Research B (22403010, 23340144, 24310010, and 25287126), and Special Funds for Education and Research (Energy Transport Processes in Geospace). This research was also partially supported by MEXT through the Grant-in-Aid for Nagoya University Global COE Program, Quest for Fundamental Principles in the Universe: From Particles to the Solar System and the Cosmos, and Inter-University Upper Atmosphere Global Observation NETwork (IUGONET). This work was also partially supported by JSPS Program for Advancing Strategic International Networks to Accelerate the Circulation of Talented Researchers under grant number G2602. This research was also partly supported by the National Institute of Polar Research through General Collaboration Projects no. 24-10. S. Nozawa thanks the International Space Science Institute (ISSI) for sponsoring the team (no. 217) meetings.

The topical editor S. Milan thanks the two anonymous referees for help in evaluating this paper.

References

Allen, C. W.: Astrophysical Quantities, 2nd edition, Athlone Press, Univ. of London, 118–123, 1963.

Arras, C., Wickert, J., Beyerle, G., Heise, S., Schmidt, T., and Jacobi, C.: A global climatology of ionospheric irregularities derived from GPS radio occultation, Geophys. Res. Lett., 35, L14809, doi:10.1029/2008GL034158, 2008.

Aso, T., Tsuda, T., and Kato, S.: Meteor radar observations at Kyoto University, J. Atmos. Terr. Phys., 41, 517–525, 1979.

Batista, P. P., Clemesha, B. R., Batista, I. S., and Simonich, D. M.: Characteristics of the sporadic sodium layers observed at 23° S, J. Geophys. Res., 94, 15349–15358, 1989.

Batista, P. P., Clemesha, B. R., Simonich, D. M.: Horizontal structures in sporadic sodium layers at 23° S, Geophys. Res. Lett., 18, 1027–1030, 1991.

Bedey, D. F. and Watkins, B. J.: Large-scale transport of metallic ions and the occurrence of thin layers in the polar ionosphere, J. Geophys. Res., 102, 9675–9681, 1997.

Bedey, D. F. and Watkins, B. J.: Diurnal occurrence of thin metallic ion layers in the high-latitude ionosphere, Geophys. Res. Lett., 25, 3767–3770, 1998.

Bedey, D. F. and Watkins, B. J.: Simultaneous observations of thin ion layers and the ionospheric electric field over Sondrestrom, J. Geophys. Res., 106, 8169–8183, 2001.

Bilitza, D.: International reference ionosphere 2000, Radio Sci., 36, 261–275, 2001.

Clemesha, B. R.: Sporadic neutral metal layers in the mesosphere and lower thermosphere, J. Atmos. Terr. Phys., 57, 725–736, 1995.

Clemesha, B. R., Kirchhoff, V. W. J. H., Simonich, D. M., and Takahashi, H.: Evidence of an extra-terrestrial source for the mesospheric sodium layer, Geophys. Res. Lett., 5, 873–876, 1978.

Clemesha, B. R., Batista, P. P., and Simonich, D. M.: Concerning the origin of enhanced sodium layers, Geophys. Res. Lett., 15, 1267–1270, 1988.

Clemesha, B. R., Batista, P. P., and Simonich, D. M.: An evaluation of the evidence for ion recombination as a source of sporadic neutral layers in the lower thermosphere, Adv. Space Res., 24, 547–556, 1999.

Cox, R. M. and Plane, J. M. C.: An ion-molecule mechanism for the formation of neutral sporadic Na layers, J. Geophys. Res., 103, 6349–6359, doi:10.1029/97JD03376, 1998.

Delgado, R., Friedman, J. S., Fentzke, J. T., Raizada, S., Tepley, C. A., and Zhou, Q.: Sporadic metal atom and ion layers and their connection to chemistry and thermal structure in the mesopause region at Arecibo, J. Atmos. Sol. Terr. Phys., 74, 11–23, 2012.

Fan, Y. Z., Plane, J. M. C., and Gumbel, J.: On the global distribution of sporadic sodium layers, Geophys. Res. Lett., 34, L15808, doi:10.1029/2007GL030542, 2007.

Folkestad, K., Hagfors, T., and Westerlund, S.: EISCAT: An updated description of technical characteristics and operational capabilities, Radio Sci., 18, 867–879, doi:10.1029/RS018i006p00867, 1983.

Gardner, C. S., Kane, T. J., Senft, D. C., Qian, J., and Papen, G. C.: Simultaneous observations of sporadic E, Na, Fe, and Ca^+ layers at Urbana, Illinois: Three case studies, 98, 16865–16873, 1993.

Gu, Y. Y., Qian, J., Papen, G. C., Swenson, G. R., and Espy, P. J.: Concurrent observations of auroral activity and a large sporadic sodium layer event during ANLC-93, Geophys. Res. Lett., 22, 2805–2808, 1995.

Hall, C. M., Aso, T., Tsutsumi, M., Nozawa, S., Manson, A. H., and Meek, C. E.: A comparison of mesosphere and lower thermosphere neutral winds as determined by meteor and medium-frequency radar at 70° N, Radio Sci., 40, RS4001, doi:10.1029/2004RS003102, 2005.

Hansen, G. and von Zahn, U.: Sudden sodium layers in polar latitudes, J. Atmos. Terr. Phys., 52, 585–608, 1990.

Hedin, A. E.: Extension of the MSIS Thermospheric Model into the Middle and Lower Atmosphere, J. Geophys. Res. 96, 1159–1172, 1991.

Heinselman, C. J.: Auroral effects on the gas phase chemistry of meteoric sodium, J. Geophys. Res., 105, 12181–12192, 2000.

Heinselman, C. J., Thayer, J. P., and Watkins, B. J.: A high-latitude observations of sporadic sodium and sporadic *E*-layer formation, Geophys. Res. Lett., 25, 3059–3062, 1998.

Kane, J. T., Hostetler, C. A., and Gardner, C. S.: Horizontal and vertical structure of the major sporadic sodium layer events observed during ALOHA-90, Geophys. Res. Lett., 18, 1365–1368, 1991.

Kane, T. J., Gardner, C. S., Zhou, Q., Mathews, J. D., and Tepley, C. A.: Lidar, radar and airglow observations of a prominent sporadic Na/sporadic E layer event at Arecibo during AIDA-89, J. Atmos. Terr. Phys., 55, 499–511, 1993.

Keay, C. S. and Ceplecha, Z.: Rate of observation of electrophonic meteor fireballs, J. Geophys. Res., 99, 13163–13165, 1994.

Kelley, M. C.: The Earth's ionosphere: Plasma physics and electrodynamics, 2nd edition, Academic Press Inc., San Diego, California, 27–70, 2009.

Kirkwood, S. and von Zahn, U.: On the role of auroral electric fields in the formation of low altitude sporadic-E and sudden sodium layers, J. Atmos. Terr. Phys., 53, 389–407, 1991.

Liu, Y. and Fan Yi, Behavior of sporadic Na layers on small time scale, J. Atmos. Sol. Terr. Phys., 71, 1374–1382, 2009.

Mathews, J. D.: Sporadic E: current views and recent progress, J. Atmos. Sol. Terr. Phys., 60, 413–435, 1998.

Matuura, N., Tsuda, T., and Nozawa, S.: Field-aligned current loop model on formation of sporadic metal layers, J. Geophys. Res., 118, 1–12, doi:10.1002/jgra.50414, 2013.

Nagasawa, C. and Abo, M.: Lidar observations of a lot of sporadic sodium layers in mid-latitude, Geophys. Res. Lett., 22, 263–266, 1995.

Nozawa, S., Kawahara, T. D., Saito, N., Hall, C. M., Tsuda, T. T., Kawabata, T., Wada, S., Brekke, A., Takahashi, T., Fujiwara, H., Ogawa, Y., and Fujii, R.: Variations of the neutral temperature and sodium density between 80 and 107 km above Tromsø during the winter of 2010–2011 by a new solid-state sodium lidar, J. Geophys. Res., 119, 441–451, doi:10.1002/2013JA019520, 2014.

Oyama, S., Kurihara, J., Watkins, B. J., Tsuda, T. T., and Takahashi, T.: Temporal variations of the ion-neutral collision frequency from EISCAT observations in the polar lower ionosphere during periods of geomagnetic disturbances, J. Geophys. Res., 117, A05308, doi:10.1029/2011JA017159, 2012.

Plane, J. M. C.: A time-resolved model of the mesospheric Na layer: constraints on the meteor input function, Atmos. Chem. Phys., 4, 627–638, doi:10.5194/acp-4-627-2004, 2004.

Qian, J., Gu, Y., and Gardner, C. S.: Characteristics of the Sporadic Na layers observed during the Airborne Lidar and Observations of Hawaiian Airglow/Airborne Noctilucent Cloud (ALOHA/ANLC-93 campaigns, J. Geophys. Res., 103, 6333–6347, 1998.

Rees, M. H.: Auroral Ionization and Excitation by Incident Energetic Electrons, Plant. Space Sci., 11, 1209–1218, 1963.

She, C. Y. and Yu, J. R.: Doppler-free saturation fluorescence spectroscopy of Na atoms for atmospheric application, App. Opt., 34, 1063–1075, 1995.

She, C. Y., Latifi, H., Yu, J. R., Alvarez II, R. J., Bills, R. E., and Gardner, C. S.: Two-frequency lidar technique for mesospheric Na temperature measurements, Geophys. Res. Lett., 17, 929–932, 1990.

Simonich, D., Clemesha, B., and Batista, P. P.: Sporadic sodium layers and the average vertical distribution of atmospheric sodium, Adv. Space Res., 35, 1976–1980, 2005.

Tsuda, T. T., Nozawa, S., Kawahara, T. D., Kawabata, T., Saito, N., Wada, S., Ogawa, Y., Oyama, S., Hall, C. M., Tsutsumi, M., Ejiri, M. K., Suzuki, S., Takahashi, T., and Nakamura, T.: Decrease in sodium density observed during auroral particle precipitation over Tromsø, Norway, Geophys. Res. Lett., 40, 4486–4490, doi:10.1002/grl.50897, 2013.

Tsutsumi, M., Holdsworth, D., Nakamura, T., and Reid, I.: Meteor observations with an MF radar, Earth Planets Space, 51, 691–699, 1999.

von Zahn, U. and Hansen, T. L.: Sudden neutral sodium layers : a strong link to sporadic E layers, J. Atmos. Terr. Phys., 50, 93–104, 1988.

von Zahn, U., der Gathen, P., and Hansen, G.: Forced release of sodium from upper atmospheric dust particles, Geophys. Res. Lett., 14, 76–79, 1987.

Whitehead, J. D.: Recent work on mid-latitude and equatorial sporadic-E, J. Atmos. Terr. Phys., 51, 401–424, 1989.

Wu, D. L., Ao, C. O., Haiji, G. A., de la T. Juarez, M., and Mannucci, A. J.: Sporadic *E* morphology from GPS-CHAMP radio occultation, J. Geophys. Res., 110, A01306, doi:10.1029/2004JA010701, 2005.

Yuan, T., Wang, J., Cai, X., Sojka, J., Rice, D., Oberheide, J., and Criddle, N.: Investigation of the seasonal and local time variations of the high-altitude sporadic Na layer (Na_s) formation and the associated midlatitude descending E layer (E_s) in lower E region, J. Geophys. Res., 119, 5985–5999, doi:10.1002/2014JA019942, 2014.

Zhou, Q., Mathews, J. D., and Tepley, C. A.: Aproposed temperature dependent mechanism for the formation of sporadic sodium layers, J. Atmos. Terr. Phys., 55, 513–521, 1993.